Tip of the Red Giant Branch Distances to NGC 4214, UGC 685, and UGC 5456[1]

Jesús Maíz-Apellániz[2], Lucas Cieza[3], and John W. MacKenty[2]

ABSTRACT

We have used WFPC2 VRI observations to calculate the distances to three nearby galaxies, NGC 4214, UGC 685, and UGC 5456 using the tip of the red giant branch method. Our values for NGC 4214 (2.94 ± 0.18 Mpc) and UGC 685 (4.79 ± 0.30 Mpc) are the most precise measurementes of the distances to these objects ever made. For UGC 5456 the data do not allow us to reach a decisive conclusion since there are two possible solutions, one leading towards a short distance around 3.8 Mpc and another one towards a long distance of 5.6 Mpc or more.

Subject headings: galaxies: distances and redshift — galaxies: individual (NGC 4214, UGC 685, UGC 5456) — galaxies: irregular — galaxies: stellar content

1. INTRODUCTION

In the last decade, the measurement of the tip of the red giant branch (or TRGB) has become a reliable method for measuring distances to galaxies with resolved stellar populations (Lee et al. 1993). This has been posible thanks to the very weak dependence of the absolute magnitude of the TRGB on metallicity (Da Costa & Armandroff 1990; Bellazini et al. 2001). Another advantage of this method (as opposed to the use of variable stars such as Cepheids or RR Lyrae) is that only a single epoch is needed to estimate the distance, considerably reducing the amount of observing time required and avoiding scheduling problems. Its robustness has been recently tested by obtaining consistent distances to the SMC, LMC, and IC 1613 using four different methods: Cepheids, RR Lyrae, red clump, and TRGB (Dolphin et al. 2001b). The use of HST/WFPC2 data allows the measurement of distances up to ≈ 5 Mpc with a single orbit using the TRGB (Karachentsev et al.

2001; Tosi et al. 2001; Dolphin et al. 2001a) and the introduction of ACS will extend that range in distance by a factor of two.

The method for using the TRGB as a standard candle has been described by Sakai et al. (1996). One constructs a smoothed version of the luminosity function in the Cousins I passband as:

$$\Phi(I) = \sum_{i=1}^{N} \frac{1}{\sqrt{2\pi}\sigma_i} \exp\left[-\frac{(I_i - I)^2}{2\sigma_i^2}\right], \tag{1}$$

where I_i and σ_i are the magnitude and photometric uncertainty of the ith star, respectively, and N is the total number of stars in the sample. We then define an adaptive edge-detection filter as:

$$E(I) = \Phi(I + \bar{\sigma}_m) - \Phi(I - \bar{\sigma}_m), \tag{2}$$

where $\bar{\sigma}_m$ is the mean photometric uncertainty for all stars with magnitudes between $I - 0.05$ and $I + 0.05$. E can then be used as a localized slope estimator to find the cutoff in the I band luminosity function created by the TRGB.

The three objects in this paper (NGC 4214, UGC 685, and UGC 5456) were selected from a study of a complete sample of galaxies from the Center for Astrophysics redshift survey (CfaRS; Huchra et al. 1983) presented by Burg (1987) [4] on the basis of their high excitation and proximity. A summary of the properties of the three galaxies is given in Table 1.

NGC 4214 is a well-studied nearby magellanic irregular galaxy. It has several intense star-forming regions concentrated along the bar of the galaxy (MacKenty et al. 2000; Maíz-Apellániz 2001) which can be easily studied thanks to the low foreground extinction and the thin character of its galactic disk (Maíz-Apellániz et al. 1999). Furthermore, the different massive young clusters are at different evolutionary stages (Maíz-Apellániz et al. 1998). These characteristics make NGC 4214 the best available template for dwarf starbursts. Leitherer et al. (1996) estimate its distance as 4.1 Mpc but they admit that the value could be lower if the distance to the Virgo Cluster is different than the one they use for their calculations. They also cite other sources' estimates ranging as high as 5.1 Mpc. On the other hand, Hopp et al. (1999) measure a distance of $\approx$ 2 Mpc using NICMOS data to find the TRGB.

UGC 685 and UGC 5456 are two smaller and less studied galaxies. They are both classified as Blue Compact Dwarfs (or BCDs) and show regions of current star formation activity, though not as intense as those in NGC 4214. Hopp (1999) and Makarova & Karachentsev (1998) find values of 5.5 Mpc and 5.9 Mpc, respectively, for the distance to UGC 685 based on the brightest

---

[4]The CfaRS consisted of 2 400 galaxies taken from the original Zwicky Catalog to a limiting magnitude of $M_B^0 = 14.5$.

blue supergiant stars. Makarova & Karachentsev (1998) also find a distance to UGC 5456 of 2.7 Mpc using the same method but specify that this value is in apparent disagreement with its radial velocity.

2.   OBSERVATIONS AND DATA REDUCTION

We obtained deep, high resolution, multiwavelength imaging of NGC 4214, UGC 685, and UGC 5456 with the WFPC2 instrument aboard HST (prop. ID 6569) on 1997 July 22, 1998 Nov 17, and 1999 Feb 18, respectively. Four continuum filters (F336W, WFPC2 U; F555W, WFPC2 V; F702W, WFPC2 wide R; and F814W, WFPC2 I) and two nebular filters (F656N, Hα and F502N, [O III] $\lambda5007$) were used for each galaxy, as shown in Table 2. The NGC 4214 nebular data and the structure of its stellar clusters were analyzed in two previous papers (MacKenty et al. 2000; Maíz-Apellániz 2001); the detailed study of the young population will be presented in a follow-up paper (Maíz-Apellániz et al. 2002). In this paper we analyze the F555W, F702W, and F814W data of the three galaxies in order to measure their distances by finding the tip of the red giant branch.

The reduction of the NGC 4214 data was described in MacKenty et al. (2000) and the reader is referred to that paper for details. The UGC 685 and UGC 5456 data were reduced in an analogous way. In particular, we point out that the F502N and F656N images were used to eliminate the nebular contribution to the F555W and F702W data, thus producing "near-pure" V and R continuum images. With one exception (the F702W filter for NGC 4214), two long and one short exposures were obtained for each filter and galaxy in order to eliminate cosmic rays and to avoid saturation at the center of compact bright sources.

We obtained the 4-band stellar photometry of each galaxy using the HSTphot package (Dolphin 2000a). HSTphot is tailored to handle the undersampled nature of the PSF in WFPC2 images and uses a self-consistent treatment of the CTE and zero-point photometric calibrations (Dolphin 2000b). The central regions of the three galaxies are dominated by a high surface density young stellar population. In those areas, blending between stars is a serious problem due to crowding and isolating the old population is not possible even at WFPC2 resolution. Therefore, we masked out those regions as well as the prominent NGC 4214 clusters identified by Maíz-Apellániz (2001). For the remaining areas, we eliminated those objects with reduced $\chi^2 > 4.0$ (poor fit: likely multiple or extended objects) and sharpness[5] < -0.3 or > 0.3 and the resulting data was grouped in three sets for each galaxy: [1] stars detected in all four filters (1 595, 325, and 197 stars for NGC 4214, UGC 685, and UGC 5456, respectively), [2] stars detected in at least F555W and F814W (13 408, 3 594, and 1 105 stars, respectively), and [3] stars detected in at least F702W and F814W (17 936, 5 207, and 1 803 stars, respectively). For each galaxy, the data in the first set were used to measure

---

[5]HSTphot defines sharpness in such a way that "perfect" stars have a value of 0, more centrally-concentrated objects (e.g. cosmic-rays) have a negative value and less-concentrated ones (e.g. galaxies) have a positive value.

extinction (as described later) while the data in the second and third sets were used to detect the tip of the red giant branch in each galaxy.

The F555W−F814W vs. F814W and F702W−F814W vs. F814W color-magnitude contour plots are shown in Figs. 4, 5, and 6. Contours are logaritmically spaced (in stars / color magnitude / brightness magnitude) in order to show the structures at both low and high densities. For each of the six possible combinations (three galaxies and two color-magnitude pairs) we performed artificial star experiments using the *hstfake* utility available in HSTphot. In each case experiments were performed in six 0.25 color-magnitudes-wide ranges and the results were interpolated for intermediate colors. In Figs. 4, 5, and 6 we show the location of the 50% completeness limit as a function of color.

3. ANALYSIS

We selected those stars with F555W−F814W between 1.0 and 3.0 in the second set and those with F702W−F814W between 0.25 and 1.5 in the third set and we built the corresponding smoothed luminosity functions in the F814W passband according to Equation 1. The values were chosen in order to maximize the number of red giants included while minimizing the number of stars of other types using Da Costa & Armandroff (1990) as a reference for $V - I$ colors and the Lejeune et al. (1997) models to transform them to $R - I$. We then calculated the corresponding edge-detection filters according to Equation 2. The results are shown in Figs. 7 and 8 and the location of the TRGB in each case is shown in Table 3. The values of Φ and E shown in Figs. 7 and 8 have been corrected for incompleteness. However, it should be noted that the incompleteness correction can become very uncertain for faint magnitudes due to small-number statistics. For that reason, we have marked in each case the location of the weighted 50% incompleteness limit. Only the data to the left of that point should be trusted when finding the TRGB.

In order to test the effects of crowding we separated the NGC 4214 data in two subsets for each of the two band sets depending on the chip where the stars were detected (PC or WF2+3+4). Since the PC has a pixel size smaller than the WF chips by a factor of 2.2, it provides a considerably better sampling of the PSF, so it should alleviate any possible crowding problems. However, we do not find any significant difference between the PC and the WF results. In all four cases a clear peak appears at essentially the same value of m_{F814W} and only for the F702W−F814W PC subset we do find a 0.3 magnitudes fainter secondary peak. Such a secondary peak would lead to an undecisive conclusion regarding the position of the TRGB if that were our only data. However, the availability of the results from the other three subsets allows us to establish the magnitude of the TRGB with precision.

For UGC 685 and UGC 5456 there are not enough stars in the PC chip to perform a similar experiment. Nevertheless, the UGC 685 data allow us to see the differences between using both sets. There are approximately twice as many stars detected in F702W and F814W than in F555W

and F814W due to two reasons: red stars are more easily detected in F702W than in F555W and the lower separation in color introduces more "blue" stars in the luminosity function. The first reason is an argument in favor of using F702W instead of F555W (more real red giants are detected) while the second one is an argument against it (more spureous objects are included in the sample), so the simultaneous use of the two sets (F555W−F814W and F702W−F814W) is a good check of the validity of the results. For UGC 685, the edge-detection filters for the two sets yield a consistent value for the TRGB which is well to the left of the 50% completeness limit, so a distance measurement can be decisively established.

Unfortunately, the same is not true for UGC 5456. A strong peak is visible in the F702W−F814W edge detection filter at $m_{\mathrm{F814W}} = 25.07$ but it is located to the right of the 50% incompleteness limit and, therefore, cannot be trusted to be real (the peak is much weaker if the incompleteness correction is not applied to Φ). A secondary peak is visible at $m_{\mathrm{F814W}} = 24.24$ in the same data set and also at $m_{\mathrm{F814W}} = 24.20$ in the F555W−F814W data set which could be caused by the TRGB but we cannot be certain about it[6]. Therefore, we conclude that UGC 5456 either is farther away than the range that can be measured with the present data or has very few red giants outside its central regions.

In order to arrive at a distance from our data there are three required steps. First, we have to correct for extinction. A minimum value for $E(B-V)$ is provided by the foreground (Galactic) value measured for the position of each galaxy by Schlegel et al. (1998) from COBE and IRAS data (see Table 4). However, the Schlegel et al. (1998) values do not take into account internal extinction within the galaxy itself. In order to measure that, we used the set with 4-band photometry and generated the three colors F336W−F555W, F555W−F702W, and F555W−F814W, We then applied an extension to > 2 colors of the standard color-color procedure (described in Maíz-Apellániz et al. 2002) to calculate the median $E(B-V)$ which affects the blue stellar population in each of the three galaxies outside the masked regions (i.e. the blue population which is approximately co-spatial with the red giants). The results are also shown in Table 4 and they are slightly higher than the values provided by Schlegel et al. (1998), as expected in the case of moderate internal extinction. Nevertheless, it is possible that some of the extinction associated with the blue population is localized around the individual stars themselves, so we will consider this second value to be an upper bound to the extinction affecting the red giant population. Therefore, we will use as our value for the extinction in each case the mean of the two results (foreground and blue population) and we will estimate the uncertainty as half the difference between them. The last column in Table 4 shows the adopted correction in the I band using a value of R_V of 3.1. Under the "other" column in Table 4 we also list the values of $E(B-V)$ measured from Balmer ratios in H II regions in the central regions of NGC 4214 and UGC 685. As expected, those values are higher

---

[6]The F555W−F814W UGC 5456 data set is a good example of one of the problems in the TRGB method: One needs to detect a large number of bright red giants in order to minimize Poisson fluctuations in Φ near the location of the TRGB. This is especially problematic when a sizable population of red super giants is present.

than the ones we use due to the considerable internal extinction present in those regions. They are shown here to serve as caution against using values obtained in such a way in similar studies of other galaxies.

The second necessary step to arrive to a distance is the conversion from WFPC2 F814W magnitudes to Cousins I ones. As described by Holtzman et al. (1995), such conversions are non-trivial for the cases of high extinction and/or certain WFPC2 filters. Fortunately, that is not the case for the galaxies analyzed here and the F814W filter. In this paper we follow Holtzman et al. (1995) and use a correction of -0.03 ± 0.01 magnitudes.

Finally, we have to choose a value for $M_{I,\mathrm{TGRB}}$. As shown by Bellazini et al. (2001), if the [Fe/H] of the studied population is known in detail, it is possible to calculate $M_{I,\mathrm{TGRB}}$ within a few hundredths of a magnitude. We do not have such a knowledge for the red giants in our galaxies but we do not really need that level of precision either, since the uncertainties from our procedure for calculating $m_{I,\mathrm{TGRB}}$ are already of the order of 0.1 magnitudes. Thus, we can settle for a value $M_{I,\mathrm{TGRB}} = 4.00 \pm 0.10$, which is valid for the range of [Fe/H] between -2.8 and -0.6 (Bellazini et al. 2001) and almost certainly includes the metallicities of the red giant population in our three galaxies.

The values for the distances are shown in Table 3. For NGC 4214, three of the four values of $m - M$ are identical so we used one of those for our adopted distance as well as the smallest of the three uncertainties (the values are not completely independent from the statistical point of view so there is no easy way to reduce the estimated uncertainty by combining them). For UGC 685 we used the values obtained with the F702W−F814W data simply because of the larger number of stars in the sample but, alternatively, the F555W−F814W result of 4.61 ± 0.30 Mpc could also be used (the distance between them is of only 0.6σ). Finally, as previously mentioned, no decisive result could be obtained for UGC 5456 so two possible values are listed.

Our distance for NGC 4214 (2.94 ± 0.18 Mpc) is in the middle of the range previously obtained by other authors (2.0 to 5.1 Mpc) but no compatibility analysis can be provided since the sources do not provide uncertainty estimates. Our distance for UGC 685 (4.79 ± 0.30 Mpc) is also quite close to the previous values available from the literature (5.5 Mpc, Hopp 1999, and 5.9 Mpc, Makarova & Karachentsev 1998). Our result is well within the uncertainty specified by the first of those articles, which is 30% (the second paper does not provide an uncertainty estimate). On the other hand, the previously value available for UGC 5456 (2.7 Mpc, Makarova & Karachentsev 1998) can certainly be excluded with our data; that galaxy is farther away, though we are not sure by how much. It is interesting to note that the previous values for the distances to UGC 685 and UGC 5456 were obtained using the same method, the magnitude of the brightest blue supergiant stars. Why would the method be valid for the first galaxy but not for the second? The explanation we prefer is that the brightest young clusters in UGC 685 are Scaled OB Associations while those in UGC 5456 are Super Star Clusters (or at least compact clusters), as described by Maíz-Apellániz (2001). Therefore, the brightest point-like sources detected from the ground in B in UGC 685

are likely to be individual blue supergiants or small aggregrates of them. On the other hand, the brightest point-like sources in UGC 5456 are clusters made out of many young stars, and confusing them with blue supergiants leads to a large underestimation of the distance.

REFERENCES

Bellazini, M., Ferraro, F. R., & Pancino, E. 2001, ApJ, 556, 635

Burg, R. I. 1987, Ph.D. thesis, Massachusetts Institute of Technology

Da Costa, G. S., & Armandroff, T. E. 1990, AJ, 100, 162

Dolphin, A. E. 2000a, PASP, 112, 1383

Dolphin, A. E. 2000b, PASP, 112, 1397

Dolphin, A. E., et al. 2001a, MNRAS, 324, 249

Dolphin, A. E., et al. 2001b, ApJ, 550, 554

Holtzman, J., Burrows, C. J., Casertano, S., Hester, J. J., Trauger, J. T., Watson, A. M., & Worthey, G. 1995, PASP, 107, 1065

Hopp, U. 1999, A&AS, 134, 317

Hopp, U., Schulte-Ladbeck, R. E., Greggio, L., & Crone, M. M. 1999, in ASP Conf. Series Proc., Vol. 192, 85

Huchra, J. P., Davis, M., Latham, D., & Tonry, J. 1983, ApJS, 52, 89

Jansen, R. A., Fabricant, D., Franx, M., & Caldwell, N. 2000, ApJS, 126, 331

Karachentsev, I. D., & Makarov, D. A. 1996, AJ, 111, 794

Karachentsev, I. D., et al. 2001, A&A, 375, 359

Lee, M. G., Freedman, W. L., & Madore, B. F. 1993, ApJ, 417, 553

Leitherer, C., Vacca, W., Conti, P. S., Filippenko, A. V., Robert, C., & Sargent, W. L. W. 1996, ApJ, 465, 717

Lejeune, T., Buser, R., & Cuisinier, F. 1997, A&AS, 125, 229

MacKenty, J. W., Maíz-Apellániz, J., Pickens, C. E., Norman, C. A., & Walborn, N. R. 2000, AJ, 120, 3007

Maíz-Apellániz, J. 2001, ApJ, in press, available from `http://www.stsci.edu/~jmaiz`

Maíz-Apellániz, J., Cieza, L., & MacKenty, J. W. 2002, AJ, submitted

Maíz-Apellániz, J., Mas-Hesse, J. M., Muñoz-Tuñón, C., Vílchez, J. M., & Castañeda, H. O. 1998, A&A, 329, 409

Maíz-Apellániz, J., Muñoz-Tuñón, C., Tenorio-Tagle, G., & Mas-Hesse, J. M. 1999, A&A, 343, 64

Makarova, I. N., & Karachentsev, I. D. 1998, A&AS, 133, 181

Sakai, S., Madore, B. F., & Freedman, W. L. 1996, ApJ, 461, 713

Schlegel, D. J., Finkbeiner, D. P., & Davis, M. 1998, ApJ, 500, 525

Tosi, M., Sabbi, E., Bellazini, M., Aloisi, A., Greggio, L., Leitherer, C., & Montegriffo, P. 2001, AJ, 122, 1271

Table 1. Reference data for the three galaxies. All data was obtained from NED with the only exception of $v_{\rm LG}$, the velocity with respect to the Local Group of galaxies, which was calculated from the heliocentric velocity, $v_{\rm helio}$ (obtained from NED), and the information provided by Karachentsev & Makarov (1996). Coordinates correspond to the J2000.0 epoch.

	NGC 4214	UGC 685	UGC 5456
RA	$12^{\rm h}15^{\rm m}38\overset{\rm s}{.}9$	$01^{\rm h}07^{\rm m}22\overset{\rm s}{.}4$	$10^{\rm h}07^{\rm m}19\overset{\rm s}{.}6$
dec	$+36°19'40''$	$+16°41'02''$	$+10°21'46''$
$v_{\rm helio}$	291 km s^{-1}	157 km s^{-1}	544 km s^{-1}
$v_{\rm LG}$	295 km s^{-1}	351 km s^{-1}	377 km s^{-1}
diameters	$8\overset{'}{.}5 \times 6\overset{'}{.}6$	$1\overset{'}{.}2 \times 0\overset{'}{.}9$	$1\overset{'}{.}6 \times 0\overset{'}{.}8$
m_B	10.20 ± 0.16	14.23 ± 0.18	13.52 ± 0.18

Table 2.   Observations.

Filter	Band	Galaxy	Images	Exp. time (s)
F656N	Hα	NGC 4214	u3n8010fm + gm	800 + 800
		UGC 685	u3n8030fr + gr	800 + 800
		UGC 5456	u3n8020fr + gr	400 + 400
F502N	[O III] λ5007	NGC 4214	u3n8010dm + em	700 + 800
		UGC 685	u3n8030dr + er	700 + 800
		UGC 5456	u3n8020dr + er	500 + 600
F336W	WFPC2 U	NGC 4214	u3n80101m + 2m + 3m	260 + 900 + 900
		UGC 685	u3n80301r + 2r + 3r	300 + 900 + 900
		UGC 5456	u3n80208r + 9r + ar	300 + 1 000 + 1 000
F555W	WFPC2 V	NGC 4214	u3n80104m + 5m + 6m	100 + 600 + 600
		UGC 685	u3n80304r + 5r + 6r	100 + 500 + 500
		UGC 5456	u3n80207r + br + cr	100 + 500 + 500
F702W	WFPC2 wide R	NGC 4214	u3n80107m + 8m	500 + 500
		UGC 685	u3n80307r + 8r + 9r	100 + 500 + 500
		UGC 5456	u3n80201r + 2r + 3r	100 + 500 + 500
F814W	WFPC2 I	NGC 4214	u3n8010am + bm + cm	100 + 600 + 600
		UGC 685	u3n8030ar + br + cr	100 + 600 + 600
		UGC 5456	u3n80204r + 5r + 6r	100 + 600 + 600

Table 3.   Results for the three galaxies. In each case the position and uncertainty of the TRGB, $m_{\mathrm{F814W,TRGB}}$, is given using both F555W−F814W and F702W−F814W data to discriminate between red and blue stars. The value of $m_{\mathrm{F814W,TRGB}}$ does not include the extinction and filter transformation corrections. For NGC 4214, results are shown both for the PC and the WF fields. The last column shows the proposed distance for the galaxies. As described in the text, the location of the TRGB for UGC 5456 cannot be conclusively determined from the data and the two possible locations lead to two different distances to the galaxy.

Galaxy	Chip(s)	F555W−F814W		F702W−F814W		Distance
		$m_{\mathrm{F814W,TRGB}}$	$m - M$	$m_{\mathrm{F814W,TRGB}}$	$m - M$	(Mpc)
NGC 4214	PC	23.48 ± 0.06	27.34 ± 0.13	23.48 ± 0.04	27.34 ± 0.13	
	WF	23.45 ± 0.13	27.31 ± 0.18	23.48 ± 0.10	27.34 ± 0.16	2.94 ± 0.18
UGC 685	All	24.48 ± 0.10	28.32 ± 0.14	24.56 ± 0.13	28.40 ± 0.14	4.79 ± 0.30
UGC 5456	All	$24.20 \pm 0.14?$	$27.87 \pm 0.28?$	$24.24 \pm 0.10?$	$27.91 \pm 0.27?$	$3.82 \pm 0.48?$
				$\gtrsim 25.07?$	$\gtrsim 28.74?$	$\gtrsim 5.60?$

Table 4.   Measured values, literature data, and adopted values for the extinction. Our measured
values are obtained from WFPC2 $UVRI$ photometry of early-type stars.

Galaxy	$E(B-V)$			Adopted A_I
	measured	SFD98[a]	other	
NGC 4214	0.09	0.02	$0.0 - 0.6^b$	0.11 ± 0.07
UGC 685	0.08	0.06	0.23^c	0.13 ± 0.02
UGC 5456	0.27	0.04		0.30 ± 0.22

[a] Schlegel et al. (1998)

[b] Maíz-Apellániz et al. (1998)

[c] Jansen et al. (2000)
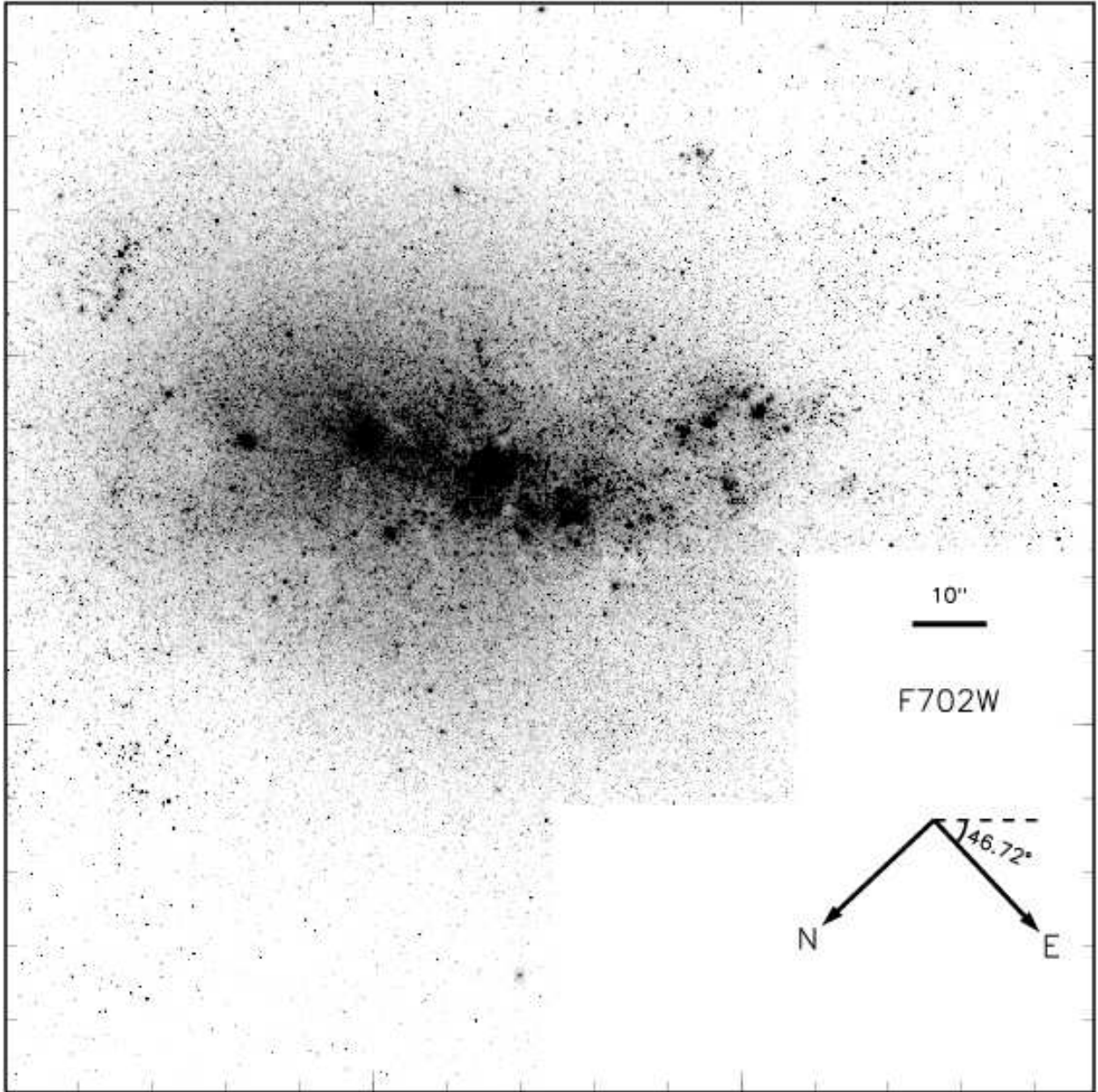
Fig. 1.— Hα subtracted WFPC2 wide R image of NGC 4214. Tick marks are shown for every hundredth pixel.
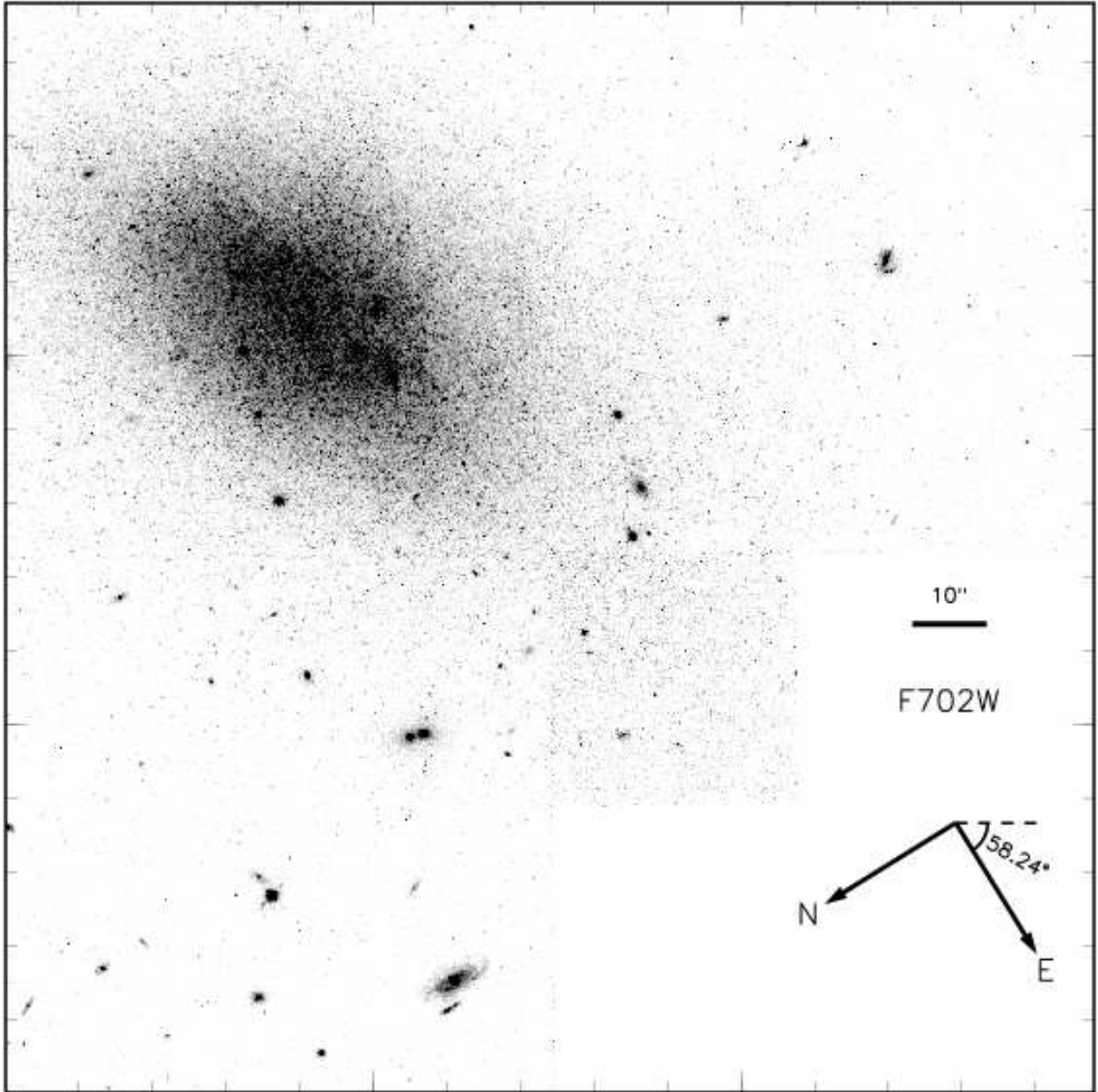
Fig. 2.— Hα subtracted WFPC2 wide R image of UGC 685. Tick marks are shown for every hundredth pixel.
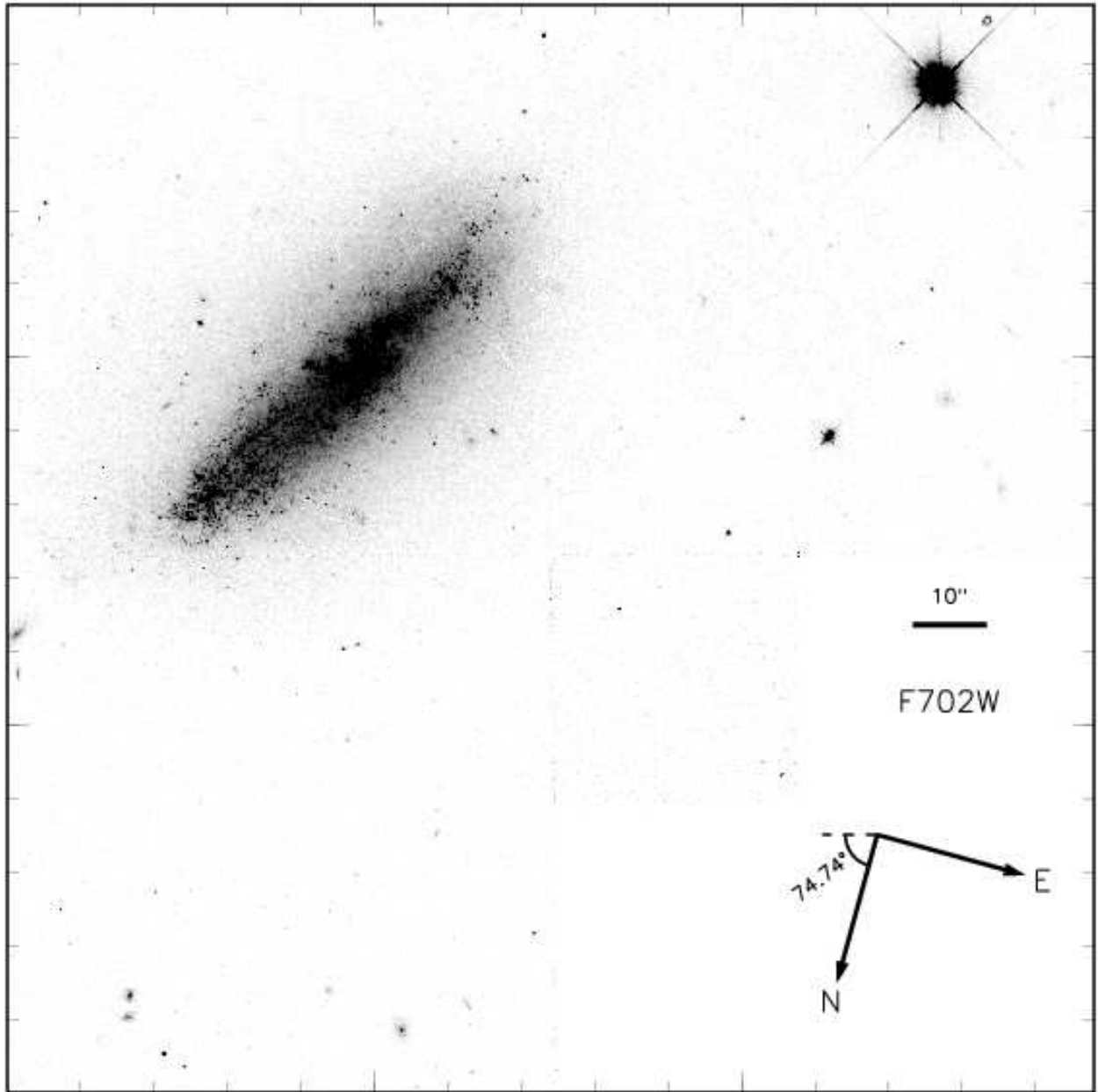
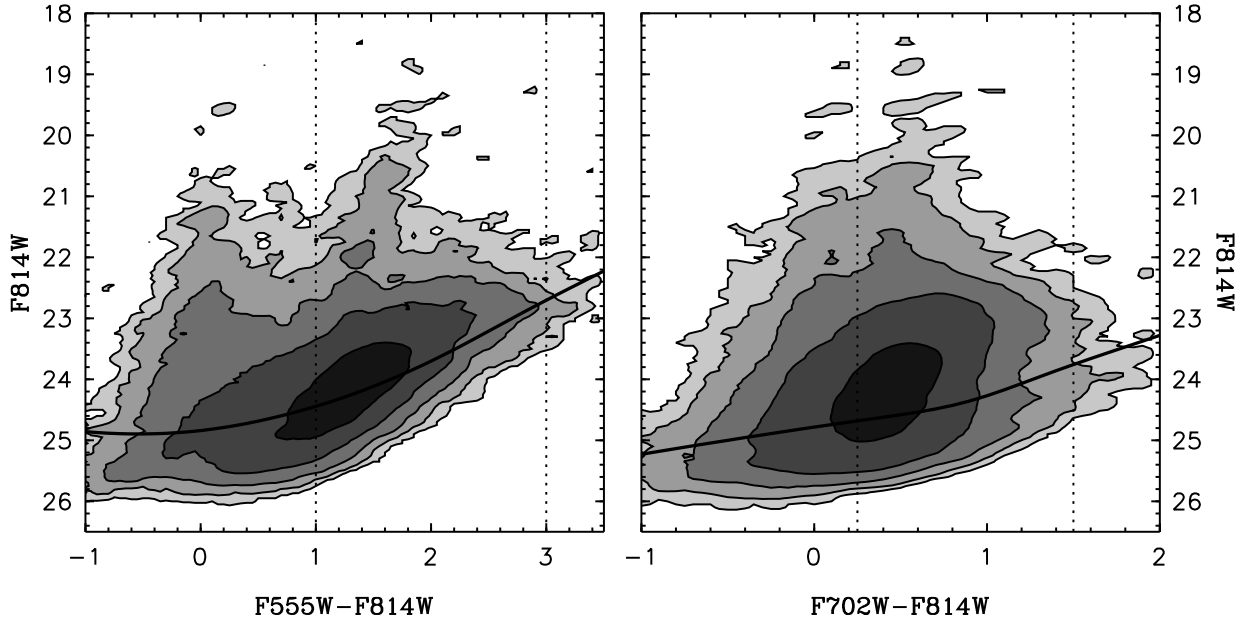Fig. 3.— Hα subtracted WFPC2 wide R image of UGC 5456. Tick marks are shown for every hundredth pixel.

Fig. 4.— Observed color-magnitude contour plots of NGC 4214. Stars in the central regions and in prominent young clusters are excluded in order to reduce blending and enhance the old population. Contours are logarithmically spaced. The thick solid line marks the 50% completeness limit but the plots themselves are not corrected for that effect. The vertical dashed lines indicate the color range used to determine the location of the tip of the red giant branch.
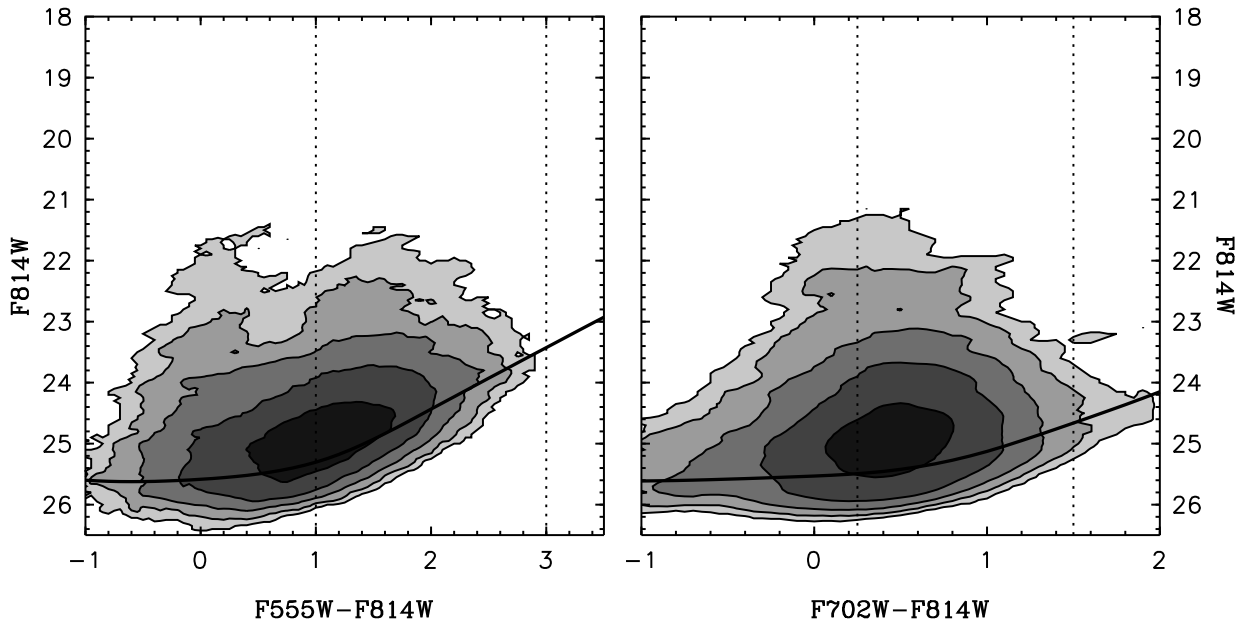
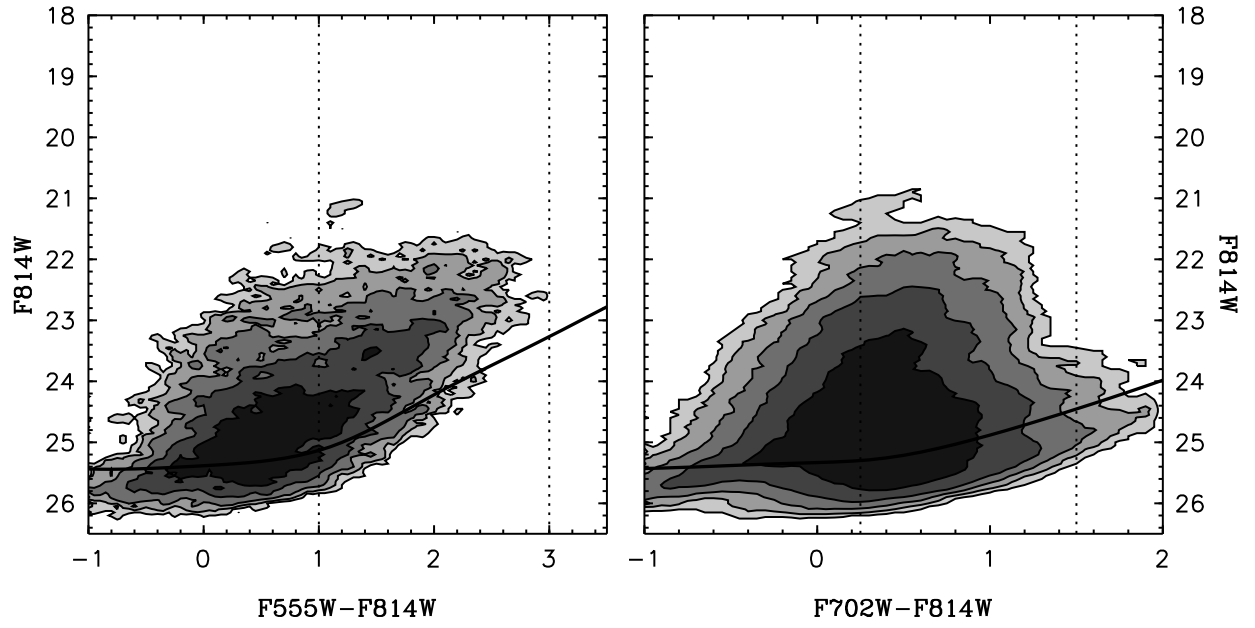Fig. 5.— Same as Fig. 4 for UGC 685.
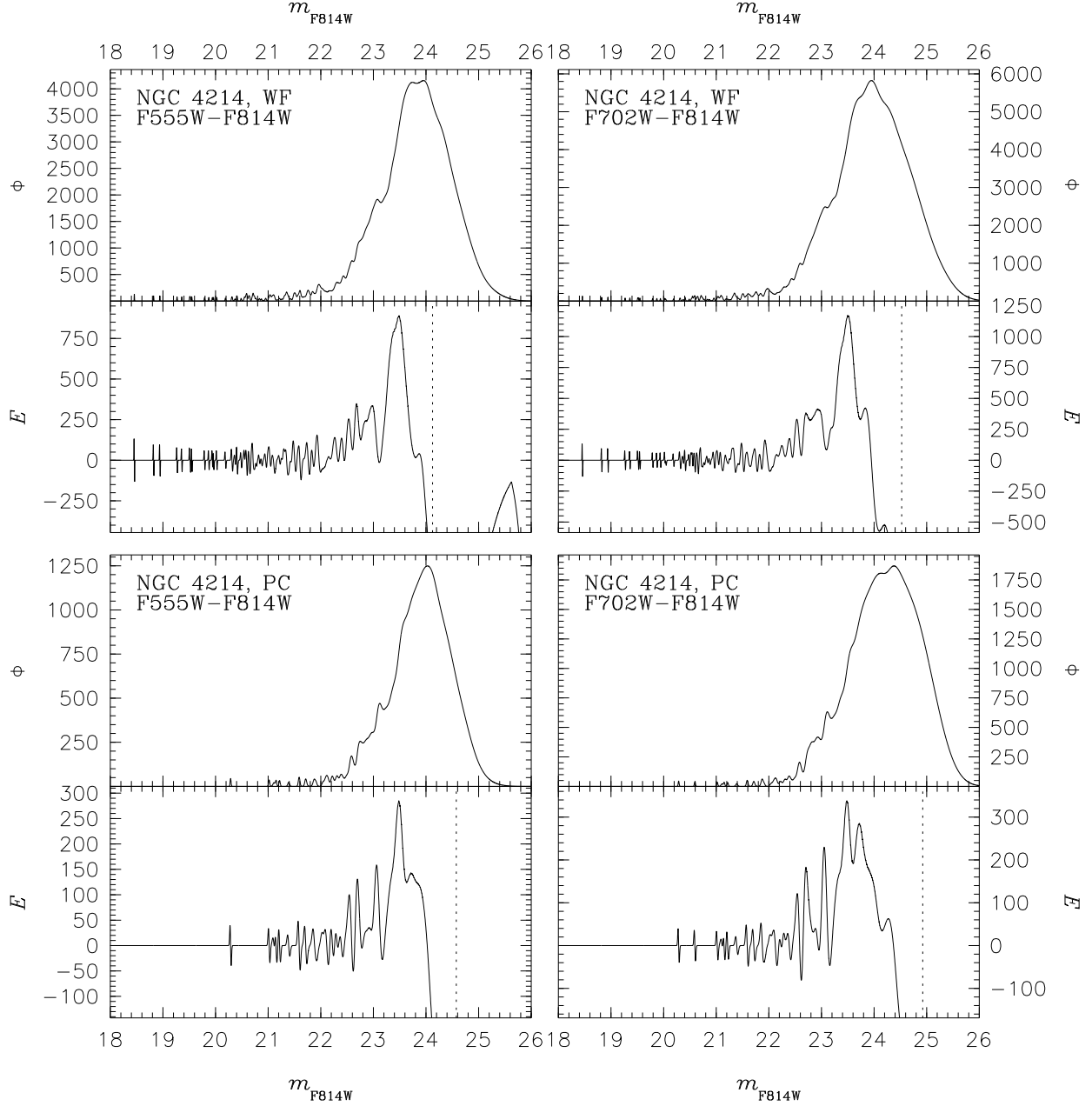
Fig. 6.— Same as Fig. 4 for UGC 5456.

Fig. 7.— F814W luminosity functions with the corresponding outputs of the edge-detection filter for NGC 4214. The upper plots are for the non-masked regions in the WF chips while the lower ones are for the PC chip. The left plots use the F555W data for the color information while the right ones use the F702W data. The dashed vertical line marks the 50% completeness in each case.
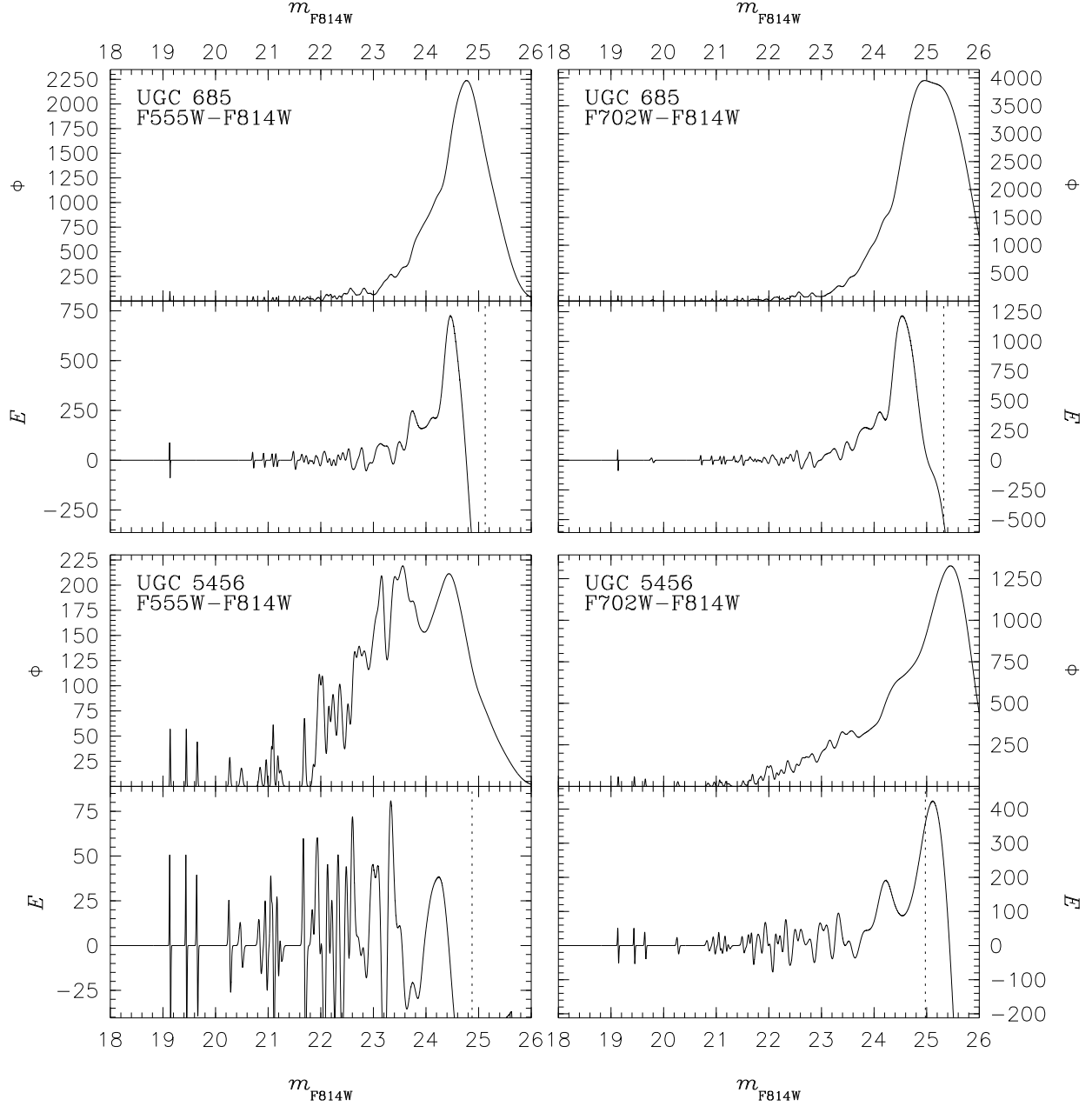
Fig. 8.— F814W luminosity functions with the corresponding outputs of the edge-detection filter for UGC 685 (upper plots) and UGC 5456 (lower plots). The left plots use the F555W data for the color information while the right ones use the F702W data. The dashed vertical line marks the 50% completeness in each case.